Journal of Organometallic Chemistry 951 (2021) 122008

Contents lists available at ScienceDirect

Journal of Organometallic Chemistry

journal homepage: www.elsevier.com/locate/jorganchem

Modulating the electronics of orthometalated Ru^{II}-NHC complexes *via* substitution patterns or NHC donors: Studies towards the impacts in catalysis

Praseetha Mathoor Illam[1], Vivek Kumar Singh[1], Priya, Arnab Rit*

Department of Chemistry, Indian Institute of Technology Madras, Chennai 600036, India

ARTICLE INFO

Article history:
Received 28 May 2021
Revised 12 July 2021
Accepted 27 July 2021
Available online 30 July 2021

Keywords:
N-heterocyclic carbene
ruthenium
orthometalation
electronic tuning
acceptorless dehydrogenation
transfer hydrogenation

ABSTRACT

The effect of electronic modulations on a series of C∧C orthometalated Ru^{II}-NHC complexes **2**-**10** was explored in (de)hydrogenation reaction. The electronic tweaking of the complexes was achieved either by varying the carbene donors (ImNHC *vs* 1,2,4-TzNHC) or the nature and position of the substituents on the N-phenyl wingtip of the NHC ligand. All the synthesized new complexes were fully characterized by using NMR analyses, mass spectrometry as well as X-ray crystallography. The electronic nature of the complexes was ascertained from the electrochemical analyses in addition to $^{13}C\{^1H\}$ NMR studies. Catalytic activities of the complexes were investigated in the acceptorless dehydrogenation of 1-phenyl-1-propanol to propiophenone, and we observed that Ru^{II}-NHC complexes containing ImNHC donors outperformed their TzNHC analogues. Further, the Ru^{II}-ImNHC precatalysts with substituents at the *para*-position with respect to the imidazolium moiety exhibited an activity trend of electron deficient complexes being more active than that of the electron rich complexes. Whereas the analogous precatalysts with the substituents at *meta*-position exhibited different activity trend (electron rich complex is superior compared to the electron deficient complexes). Additionally, the complexes were also tested in the transfer hydrogenation of acetophenone and surprisingly, in contrast to dehydrogenation reaction, the *meta*-substituents had no effect on the transfer hydrogenation activities of the complexes.

1. Introduction

After the seminal report of isolable N-heterocyclic carbene (NHC) by Arduengo in 1991 [1], the organometallic chemistry involving NHCs has become an exciting area of research. Soon after this, NHCs have gained a privileged position among the ancillary ligands due to better σ-donor properties as compared to the classical ligands like amines and trisubstituted phosphines [2a,2b,2c]. Owing to the relatively easy stereoelectronic tunability and the stronger M-NHC bonds, the NHC-transition metal complexes have been widely used as efficient homogeneous catalysts for diverse organic transformations [3]. Among various NHC ligands, generally the bidentate and tridentate variants are getting more attention than their monodentate analogues possibly due to their ability to improve the stability and efficiency imparted to their metal complexes because of the chelate effect [4]. In addition, several attempts have been made to study the impact of stereoelectronic modifications of ancillary NHC ligands in the catalytic performances of their transition metal complexes. In this line, Valerga *et al.* in 2012 have reported the picolyl-functionalized orthometalated Ru^{II}-NHC complexes for the N-alkylation of amines as well as the transfer hydrogenation of carbonyl and imine moieties [5]. The stereoelectronic modifications in these complexes were achieved by changing the backbone and the wingtip of ancillary NHC ligands. Further, the electronic difference between the imidazolylidene and 1,2,4-triazolylidene donors was successfully showcased by Choudhury *et al.* in the oxidative cleavage of alkenes where the electron deficient 1,2,4-triazolylidene based precatalyst outperformed its imidazolylidene analogue [6a]. Recently, the same group has reported various stereoelectronically modifiable Ir^{III}-complexes of bidentate ImNHC ligands for the hydride transfer reaction and it was established that the yaw angle, bite angle, and the electron density at the metal centers imparted by the ligands significantly influence their catalytic performances [6b]. Along the same line, a recent report from our group described the impact of ancillary NHC ligand modifications, in terms of electronics as well as sterics, on the catalytic activity of the corresponding Ru^{II}-NHC complexes in transfer hydrogenation reaction [7a]. We have also demonstrated a similar kind of tuning in the heteroditopic NHC supported Ru^{II}-

* Correspondence author.
E-mail address: arnabrit@iitm.ac.in (A. Rit).
[1] These authors contributed equally.

https://doi.org/10.1016/j.jorganchem.2021.122008
0022-328X/

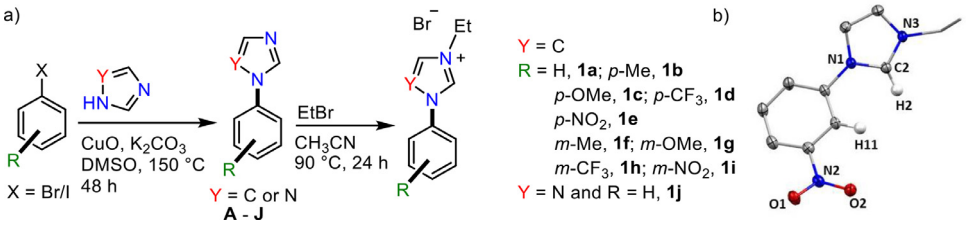

Scheme 1. a) Synthesis of various azolium salts, **1a-j** *via* Ullmann coupling protocol followed by quaternization of the azole rings. b) Molecular structure of $[\mathbf{1i}]^+$ with 60% probability level. Bromide counterion and the hydrogen atoms except H2 and H11 are omitted for clarity. The N-ethyl group is shown in capped stick.

complexes and the impact of these modulations in their catalytic activities [4b,7b]. Inspired by these results, we aimed to study the effect of such type of tuning in Ru^{II}-NHC based catalyst systems in other functional group transformations. In this line, a series of orthometalated Ru^{II}-NHC complexes were synthesized by varying the NHC donors and the substituents (including their position) at the N-phenyl wingtip group for studying their activity in the acceptorless dehydrogenation of secondary alcohol, a crucial step in various C-C and C-N bond forming reactions *via* borrowing hydrogen (BH) pathway [2d,3b], to explore the impact of the ancillary NHC ligand modulations. Additionally, the catalytic behavior of the complexes was also examined in transfer hydrogenation of carbonyl functionality.

2. Results and discussion

2.1. Synthesis of various imidazolium and triazolium salts, *1a-j*

To begin with our plan of synthesizing stereoelectronically tunable Ru^{II}-NHC complexes, various imidazolium and triazolium salts were isolated in good yields (73-89%, scheme 1). To have better insight into the electronic modulations, position (*para*-, **1b**-**e** and *meta*-, **1f**-**i**) of the substituents at the N-phenyl ring with respect to the imidazolium moiety as well as the NHC-moieties (imidazolium, **1a** *vs* triazolium, **1j**) were altered. The azolium salts **1a, 1c**, and **1d** were synthesized following the previous procedure [7a]. For the synthesis of these azolium salts, initially, the respective aryl halides were coupled with imidazole or 1,2,4-triazole *via* Ullmann coupling protocol to provide the corresponding compounds **A**-**J** which on treatment with ethyl bromide in acetonitrile under reflux condition delivered the respective azolium salts **1a-j** as off-white to yellow solids. Interestingly, the imidazolium salts with electron donating substituents (**1b**-**c** and **1f**-**g**) were found to be hygroscopic whereas the triazolium salt **1j** and other imidazolium salts with electron withdrawing substituents **1d**-**e** and **1h**-**i** were isolated as air and moisture stable solids. All these azolium salts, the precursors for NHC donors, were thoroughly characterized *via* NMR spectroscopy (see supporting information), mass spectrometry as well as by X-ray crystallography for **1i**. The presence of the downfield shifted N-C*H*-N protons and the characteristic quartets and triplets for the N-ethyl moieties in **1a-j** in their ^{1}H NMR spectra when compared to their parent compounds **A**-**J** confirmed the formation of the azolium salts.

2.2. Synthesis of the orthometalated Ru^{II}-NHC complexes *2-10*

After having the required azolium salts in our hand, we targeted the synthesis of the corresponding Ru^{II}-NHC complexes. In this direction, a series of orthometalated Ru^{II}-NHC complexes with *p*-Me (**3**) and *p*-NO_2 (**6**) as well as the *meta*-substituted complexes (**7**-**9**) were synthesized along with a 1,2,4-triazolylidene analogue **10** as shown in scheme 2.

All the complexes were isolated as air stable yellow solids in good yields (69-80%). Formation of the complexes was primarily evidenced from their ^{1}H NMR spectra where the most downfield shifted N-C*H*-N protons were absent (see supporting information). Further, the presence of four aromatic protons instead of five suggests that the metal is also attached to the phenyl ring *via* C-H activation to form ruthenacycles. Additionally, orthometalation results in the loss of symmetry around the Ru center which was supported by the splitting of *p*-cymene aromatic protons (four instead of two doublets) in the region of 5.30–5.70 ppm as well as the splitting of the N-CH_2 signals of the ethyl moiety (quartet in the azolium salts) into two multiplets [7a,8b]. To our surprise, all our attempts for the metalation of **1g** to synthesize analogous complex under various conditions ended up with the formation of a nearly 1:1 mixture of two orthometalated complexes (**11a** and **11b**, scheme 3) as evidenced from the ^{1}H NMR spectrum of the isolated product (Fig. 1).

Further, the ESI-MS spectrum of the isolated product displays only a single peak for the positive ion $[M+Na]^+$ ($M = C_{22}H_{27}N_2ORuBr$ for **11a**/**b**) with m/z = 541.0238 which is in good agreement with the calculated value (m/z = 541.0244 with the isotopic pattern matching exactly, Fig. 2). This observation reinforces the conclusion obtained from ^{1}H NMR spectrum that the metalation of **1g** results in the formation of two regioisomeric products **11a** and **11b**.

It is to be noted that the *p*-OMe substituted imidazolium salt **1c** resulted in the formation of the corresponding orthometalated complex **4** as both the *ortho*-phenyl protons with respect to the NHC moiety are equivalent. Whereas, the presence of *m*-OMe substituent somehow makes the non-equivalent *ortho*-C-H bonds reasonably electron rich and accessible for orthometalation, as supported by the experimental results (Fig. 1) in contrast to other *meta*-substituents.

The coordination of the Ru^{II}-center to the ligands in a chelating ($C_{NHC}\wedge C_{phenyl}$) fashion is further confirmed from $^{13}C\{^1H\}$ NMR spectra which show the corresponding metal bound carbene (C_{NHC}) signals as well as the C_{Phenyl} signals in their usually observed range [7a,8] as shown in Table 1. In line with previous study [7a], the new orthometalated complexes with substituents at the *para*-position, **3** and **5** also exhibited the similar trend for their $^{13}C\{^1H\}$ chemical shift values (Table 1, entry 2 and 4). The Ru^{II}-bound C_{NHC} and C_{Phenyl} chemical shift values were found to

Table 1
$^{13}C\{^1H\}$ NMR chemical shifts of the C_{NHC} and C_{Phenyl} carbons in complexes **2**-**10.**

Entry	Complex	C_{NHC} chemical shift (ppm)	C_{Phenyl} chemical shift (ppm)
1	**2**	187.0	162.4
2	**3**	186.5	162.1
3	**4**	185.4	155.7
4	**5**	188.0	163.4
5	**6**	189.2	164.7
6	**7**	187.2	157.6
7	**8**	187.5	170.1
8	**9**	187.6	181.1
9	**10**	189.3	159.6

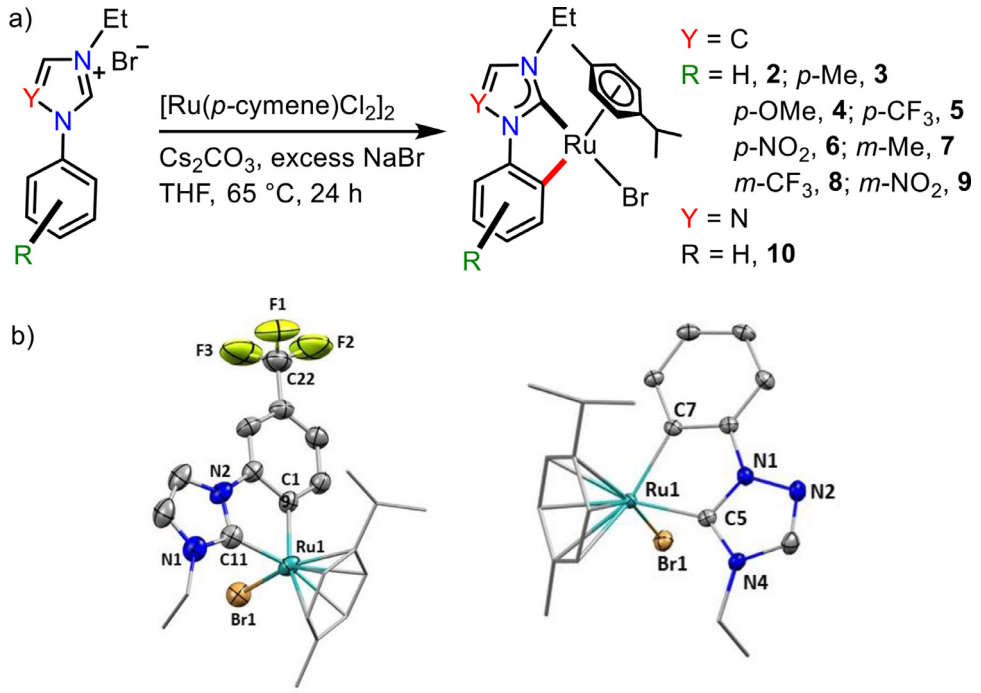

Scheme 2. a) Synthesis of the orthometalated Ru^{II}-NHC complexes **2**-**10**. b) Molecular structures of complexes **8** (left) and **10** (right) with 40% and 60% probability levels, respectively. Hydrogen atoms are omitted for clarity. N-Ethyl and *p*-cymene moieties are shown in capped stick.

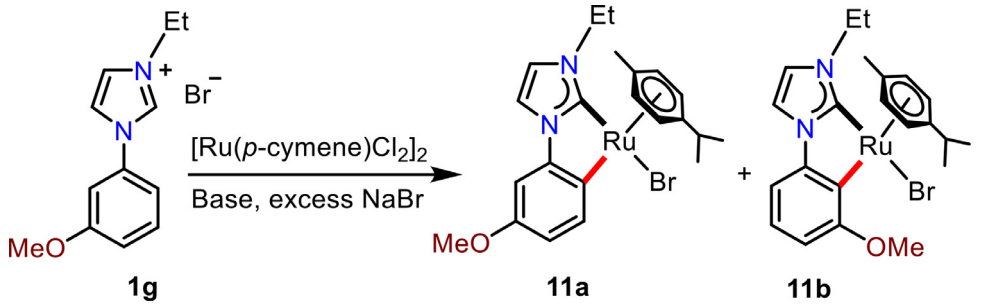

Scheme 3. Attempted synthesis of the orthometalated Ru^{II}-NHC complexes of **1g**.

be upfield shifted for complex **3** whereas those of the complex **5** were found to be downfield shifted than that of the unsubstituted complex **2** and this supports the difference in electronic nature of the NHC ligands in these complexes [7c].

In contrast to this observation, the *meta*-substituents at the N-phenyl ring with respect to the imidazolylidene ring has different influence on the $^{13}C\{^1H\}$ NMR chemical shift values of the complexes **7**-**9** (Table 1). The substituents have insignificant effect on the C_{NHC} resonances, however, they have substantial influence on the C_{Phenyl} resonances (entry 6-8 *vs* 1). The Me-substituted complex **7** has the most upfield shifted phenylic carbon signal whereas the NO_2-substituted complex **9** has the most downfield shifted phenylic carbon signal and the CF_3-substituted complex **8** has the corresponding carbon resonance value in between that observed for the complexes **7** and **9**. So, the substituents at the *para*-position influence both the C_{NHC} and C_{Phenyl} $^{13}C\{^1H\}$ NMR resonances (entry 2-5) in their orthometalated Ru^{II}-complexes. In contrast, the substituents at the *meta*-position although do not influence the respective C_{NHC} chemical shift values, the C_{Phenyl} resonance shifts substantially from their non-substituted analogue (entry 6-8 *vs* 1).

Further, the C_{Phenyl} resonance is more upfield shifted if the Me-substituent is at the *meta*-position (complex **7**) rather than at the *para*-position (complex **3**; entry 6 *vs* 2). Similarly, the C_{Phenyl} resonance is more downfield shifted in case of *m*-NO_2 substitution (complex **9**) compared to its *p*-NO_2 analogue **6** (entry 8 *vs* 5). This can be justified based on the fact that the substituents at the *meta*-position with respect to ImNHC are actually in the *para*-position of the orthometalated carbon and thus, the C_{Phenyl} chemical shift is most affected by the electron- withdrawing or donating nature of the substituents. Finally, due to the presence of an extra electronegative N-atom in 1,2,4-triazolylidene than that in the imidazolylidene, [6a,9] the complex **10** exhibited the most downfield shifted C_{NHC} resonance among all the complexes listed in Table 1.

The molecular structures of the complexes **8** and **10** were unambiguously confirmed by the X-ray diffraction studies of the single crystals obtained by the slow diffusion of *n*-pentane into the saturated DCM solutions of the complexes. The molecular structures clearly show that the NHC ligand coordinate to the Ru^{II} center in chelated fashion as concluded from their multinuclear NMR analyses. The Ru-C_{NHC} bond lengths are found to be shorter than the Ru-C_{Phenyl} lengths for both the complexes **8** and **10** possibly because of slight back donation from the Ru^{II} center to the NHC moiety [10]. Further, the Ru^{II}-C_{NHC} bond length of the complex **10** is slightly longer than the imidazolylidene complexes [2.033 *vs* 2.010 (for **2**) and 2.020 (for **8**)] and the same is also observed for the Ru-C_{Phenyl} bond length [2.089 *vs* 2.066 (for **2**) and 2.051 (for **8**)]. As a

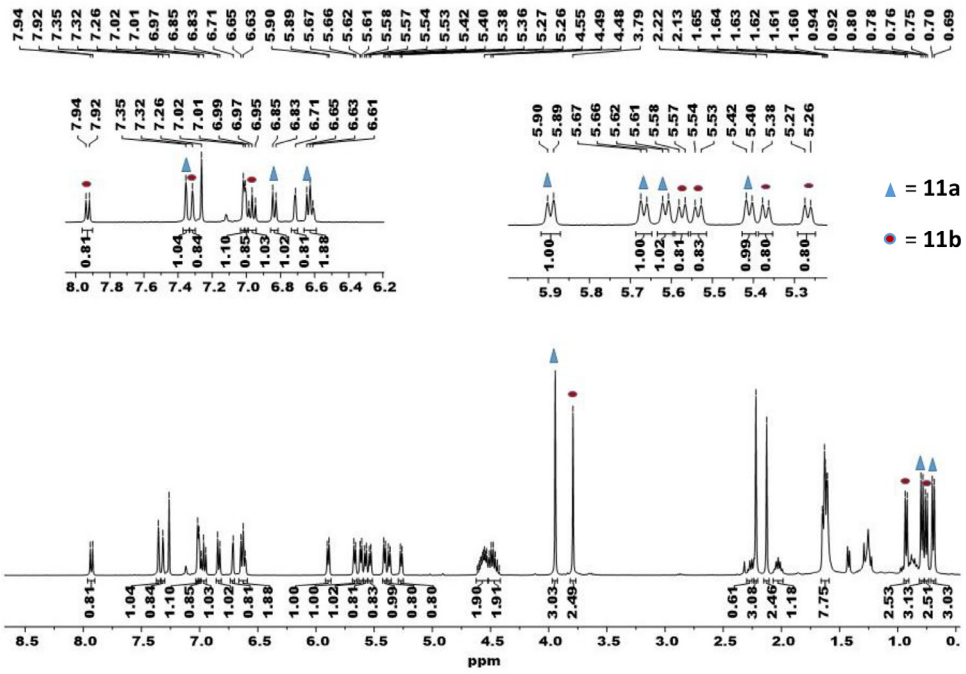

Fig. 1. ^{1}H NMR spectrum ($CDCl_3$) of the product obtained from the reaction of **1g** with [Ru(*p*-cymene)Cl_2]$_2$.

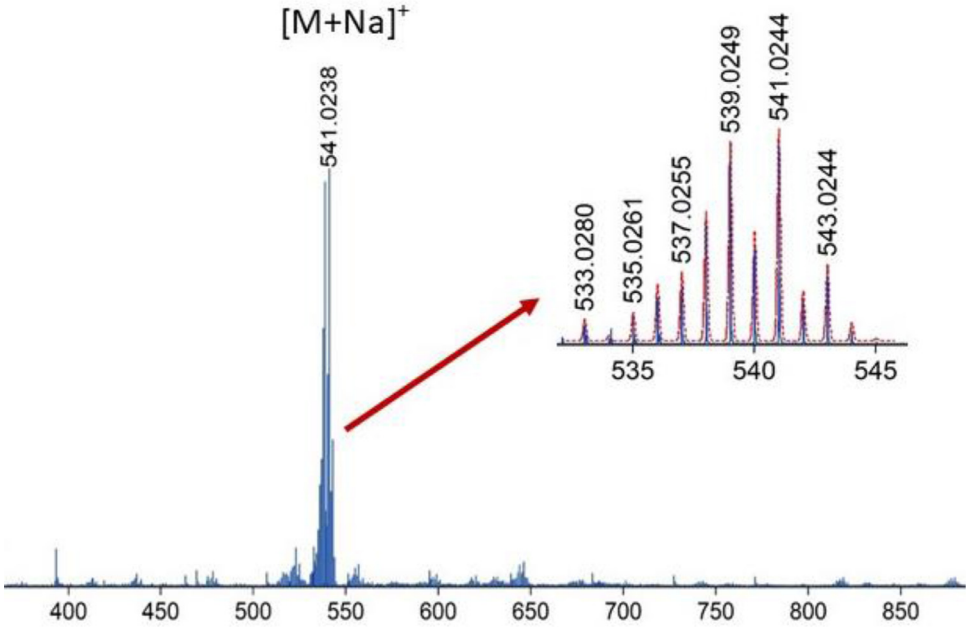

Fig. 2. ESI-MS spectrum of the product obtained from the reaction of **1g** with [Ru(*p*-cymene)Cl_2]$_2$ showing the peak at m/z = $[M+Na]^+$, M = $C_{22}H_{27}N_2ORuBr$.

measure of the steric profile of chelating ligands, the yaw and bite angles at the NHC/aryl moieties of complexes were calculated and found to be 10.60° and 77.41°, respectively for the complex **8** while 10.99° and 76.92°, respectively for the complex **10**.

More insight into the electronic nature of the synthesized complexes was obtained from their electrochemical analyses and the relevant DPV diagram is presented in Fig. 3. When the potential values of the newly synthesized *para*-substituted complexes **3** and **6** were compared with other *para*-substituted complexes **4** and **5** [7a], we observed that the electron density around the Ru center in complex **3** is lower than the analogous OMe substituted complex **4** ($E_{1/2}$ = 82.4 mV *vs* 72.0 mV) whereas the complex **6** with NO_2 substituent is more electron deficient than that of the CF_3-substituted counterpart **5** ($E_{1/2}$ = 271.3 mV *vs* 224.5 mV) in line with the higher -R effect of the NO_2-group.

The potential values obtained for the *meta*-substituted complexes reveal that the complex **7** having a Me-substituent has the highest electron density around the metal center ($E_{1/2}$ = 60.1 mV) which is also clear from the C_{Phenyl} $^{13}C\{^1H\}$ NMR chemical shift (Table 1) whereas the NO_2-substituted complex **9** is the least electron rich ($E_{1/2}$ = 285.2 mV) among the complexes analyzed. The Ru^{II}-center in the triazolylidene complex **10** is relatively more electron rich than the complexes with electron withdrawing substituents (CF_3, NO_2) either at the *para*- or *meta*- positions. All these observations imply that our simple strategy of NHC ligand modulation by varying the substitution has considerable effect

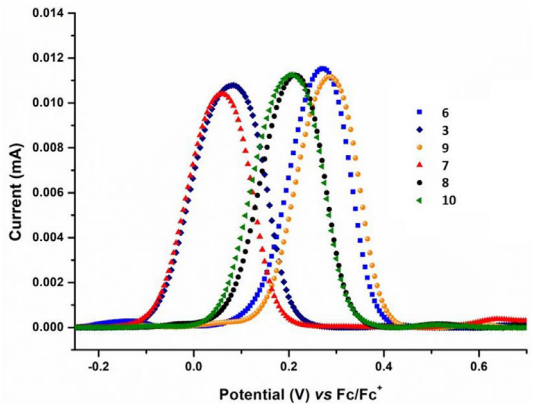

Entry	Complex	$Ru^{II/III}$ potential (mV) *vs* Fc(0/+1)
1	**3**	82.4
2	**4**	72.0
3	**5**	224.5
4	**6**	271.3
5	**7**	60.1
6	**8**	213.3
7	**9**	285.2
8	**10**	207.0

Fig. 3. DPV plot of the selected complexes. The measurements of all the Ru^{II}-NHC complexes (1 mM) were performed in degassed CH_2Cl_2 using Bu_4NPF_6 (0.1 M) as supporting electrolyte with three electrode configurations: counter electrode, Pt wire; working electrode, Glassy carbon; reference electrode, $Ag/AgNO_3$ at sweep rate of 100 mV/sec. Ferrocene ($E_{1/2}$, Fc/Fc^+ = 0.269 volts vs. Ag/Ag^+) was used as an external calibration standard for all the measurements. The potential values obtained are tabulated in the right-hand side.

Table 2
Acceptorless dehydrogenation of 1-phenyl-1-propanol using different orthometalated Ru^{II}-NHC complexes[a].

Entry	Precatalyst	Loading (mol%)	Conversion[b] (%)
1	**2**	0.5 (0.3)	97 (87)
2	**10**	0.5 (0.3)	49 (34)
3	**3**	0.3	84
4	**4**	0.3	77
5	**5**	0.3	100
6	**6**	0.3	97
7	**7**	0.3	98
8	**8**	0.3	74
9	**9**	0.3	80
10	$[Ru(p\text{-cymene})Cl_2]_2$	0.3	36

[a] General conditions: 1-phenyl-1-propanol (0.5 mmol), complex (0.3-0.5 mol%), KO^tBu (0.2 equiv.), 12 h. [b]Determined by GC-MS with respect to 1-phenyl-1-propanol.

in tuning the electronic properties of their metal complexes. Further, the above described electrochemical analyses reinforce that the substituents at the *meta*-position is more effective than the *para*-substitution (entry 2 *vs* 5 and 4 *vs* 7, Table 2) in electronic modulation of their orthometalated complexes which are also supported by the $M\text{-}C_{Phenyl}$ $^{13}C\{^1H\}$ NMR resonances (Table 1).

2.3. Catalytic acceptorless dehydrogenation of 1-phenyl-1-propanol

After having the well-characterized Ru^{II}-NHC complexes in our hand, we intended to study the effect of their electronic tuning in their catalytic activity. For that, the acceptorless dehydrogenation of 1-phenyl-1-propanol was chosen as the model reaction. The method of acceptorless dehydrogenation has gained immense attention in recent time as it is a green and atom economic way to convert the generally less reactive alcohols into more reactive carbonyl functions under the release of only molecular hydrogen [3b,11]. Importantly, it is one of the intermediate steps of the C-C and C-N bond forming reactions *via* borrowing hydrogen strategy [12].

Initially, we studied the catalytic efficacy of the basic imidazolylidene and triazolylidene complexes **2** and **10** by using KO^tBu (20 mol%) as the base in toluene solvent (Table 2). When the reaction was carried out with 0.5 mol% catalyst loading for 12 h, we observed that the complex **2** converted the 1-phenyl-1-propanol to propiophenone near quantitatively (97%, entry 1), whereas the complex **10** exhibited poor activity (entry 2, 49% conversion). When the lower catalyst loading of 0.3 mol% was employed, complex **2** still provided good conversion (87%, entry 1) but the activity of the complex **10** was further reduced (34% conversion, entry 2). To move forward, we selected the Ru^{II}-imidazolylidene complexes with varying substituents at different positions of the N-phenyl ring (complexes **3**-**9**). When the *para*-substituted complexes (**3**-**6**) were tested, the electron deficient complexes **5** and **6** performed better (97-100% conversion) than their electron rich variants (complexes **3** and **4**, 77-84%). We then checked the effect of electronic tuning by selecting the complexes with substituents at *meta*-positions (complexes **7**-**9**) and we observed a different reactivity pattern for the complexes.

The most electron rich Ru^{II}-complex **7** outperformed the analogous electron deficient complexes **8** and **9** for the conversion of 1-phenyl-1-propanol to propiophenone (entry 7, 98% *vs* 74-80%, entries 8-9). A reaction using only $[Ru(p\text{-cymene})Cl_2]_2$ (0.3 mol%) was also carried out which resulted in 36% conversion under our standard reaction conditions (entry 10) which shows that our carbene ligand is highly beneficial for improving the catalytic efficiency of the Ru^{II}-center. It is important to mention that the complexes **5**-**7** are found to be better precatalysts compared to the previously reported Ru^{II}-NHC complexes for the dehydrogenation of secondary alcohols [13a,13b,13c]. In order to understand the different reactivity patterns of the *para*- (**3**-**6**) and *meta*-substituted complexes **7**-**9**, possibly in terms of the mechanism involved, we carried out some controlled experiments. Addition of excess arenes (*p*-cymene, mesitylene and 1,3,5-trimethoxybenzene) did not alter the catalytic outcome of reactions catalyzed by the representative complexes **6** and **7** which possibly rules out the irreversible release of *p*-cymene during the catalytic process [6a,13d,13e]. Further, the mercury dropping test did not have any influence on the reaction outcome which suggests that the catalytic reaction proceeds in homogeneous fashion [13d,14]. To have better idea about the reaction mechanism, we have monitored the reaction progress using NMR spectroscopy. The ^1H NMR spectrum of the reaction mixture after stirring the *m*-methyl substituted complex **7**, KO^tBu and 1-phenyl-1-propanol for 3 h is shown in the Fig. 4. The spectrum suggests that the secondary alcohol undergoes dehydrogenation under the generation of a Ru^{II}-di-hydride intermediate, possibly by cleaving the orthometalation, as indicated by the two upfield shifted resonances of nearly equal intensity at -10.01 and -9.92 ppm. Further, the single multiplet for the methylene protons of N-ethyl wingtip group of the NHC ligand at 4.31-4.40 ppm suggests the dissociation of the $Ru\text{-}C_{Phenyl}$ bond which would make the methylene protons non-diastereotopic.

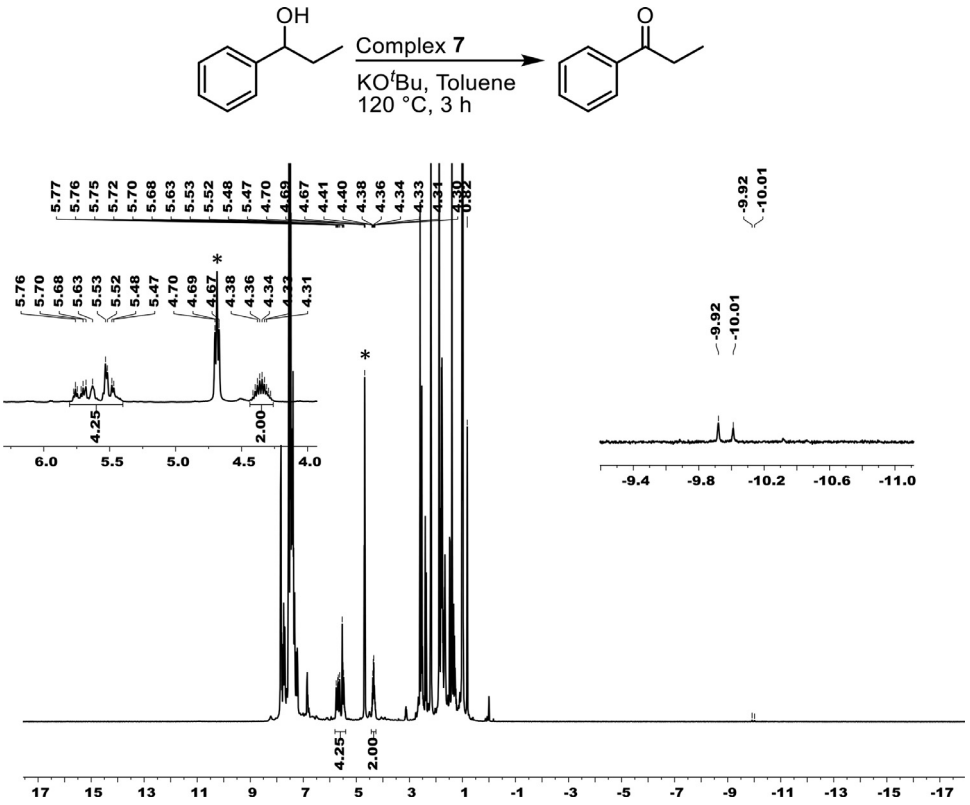

Fig. 4. In situ ^{1}H NMR spectrum of the reaction mixture (CD_3CN) for the reaction of complex **7**, KO^{t}Bu and 1-phenyl-1-propanol in toluene after 3 h. The triplet (*) corresponds to the reactant Ph(**CH**)OH(CH_2CH_3).

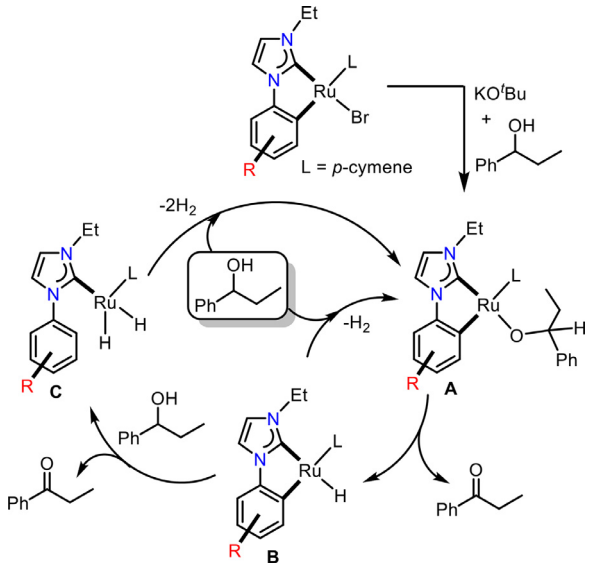

Scheme 4. Plausible reaction pathway for the acceptorless dehydrogenation of 1-phenyl-1-propanol.

In addition, the four symmetrical doublets corresponding to the *p*-cymene aromatic protons observed for the orthometalated complex **7** collapsed in the region 5.47-5.76 ppm which also supports the cleavage of the orthometalation [15]. Based on these observations, a plausible mechanistic pathway for the acceptorless dehydrogenation process has been proposed in scheme 4. At first, the base promoted deprotonation of the 1-phenyl-1-propanol followed by reaction with the Ru^{II}-NHC precatalysts generates the intermediate **A**, which upon β-hydride elimination results in the formation of a monohydride intermediate **B** under the release of propiophenone. This monohydride species might be reactive and thus may further react with 1-phenyl-1-propanol to generate a Ru^{II}-dihydride species (**C**). Further, the release of dihydrogen (see Figure S33, supporting information) from the hydride intermediate **C**/**B** *via* reaction with 1-phenyl-1-propanol continue the catalytic cycle through **A**. Involvement of the Ru^{II}-mono-hydride intermediate in the catalytic cycle was supported by the in situ ^{1}H NMR analysis of the reaction performed with the complex **5** (see Figure S32, supporting information).

2.4. Catalytic transfer hydrogenation of acetophenone

After studying the catalytic activity of the synthesized Ru^{II}-NHC complexes in acceptorless dehydrogenation process, we further investigated their activity in the reverse reaction of hydrogenation. For that, *para*- and *meta*-methyl substituted complexes **3** and **7** (keeping in mind our previous experience that electron-rich complexes perform better in hydride transfer reaction) [7a] as well as the basic ImNHC and TzNHC complexes **2** and **10**, respectively were selected and the hydrogenation of acetophenone was chosen as the model reaction under the transfer hydrogenation conditions of 10 mol% KO^{t}Bu in isopropanol (as solvent as well as hydride source). The catalytic outcomes with various complexes are shown in Table 3.

From the entry 1 and 4, it is clear that the unsubstituted complexes **2** and **10** perform similarly providing 66% (0.1 mol% loading) to ~85% (0.25 mol% loading) conversion to 1-phenylethanol. Further, with the low catalyst loading of 0.1 mol%, we observed a substantial difference in the activities between the methyl substituted (both *para*- and *meta*-) complexes **3** and **7** (entry 2-3) and the parent unsubstituted complexes (entry 1 and 4). This might be accredited to the electron richness of the Ru^{II}-center in the com-

Table 3
Transfer hydrogenation of acetophenone using complexes **2, 3, 7**, and **10**[a].

Entry	Precatalyst	Loading (mol%)	Conversion (%)[b]
1	**2**	0.25/ 0.1	86/ 66
2	**3**	0.1	83
3	**7**	0.25 / 0.1	87/ 85
4	**10**	0.25 / 0.1	84/ 66

[a] General conditions: acetophenone (1 mmol), complex (0.25-0.1 mol%), KO^{t}Bu (0.1 equiv.), 1 h. [b]Determined by GC-MS with respect to acetophenone.

plexes **3** and **7** as compared to the parent complexes **2** and **10** (Fig. 3 and Table 1). On the other hand, no considerable difference in the catalytic activities between the Me-substituted complexes **3** (with *p*-Me) and **7** (with *m*-Me) was noted (entry 2 *vs* 3). It is evident from these observations that the substituent position (*meta-vs para-*) has minimal effect on the transfer hydrogenation activity.

3. Conclusion

In summary, the catalytic behavior of various orthometalated Ru^{II}-NHC complexes, possessing different electronic natures, in acceptorless dehydrogenation reaction of 1-phenyl-1-propanol was investigated. The electronic modifications in the complexes were achieved by varying the carbene donors from ImNHC (**2**-**9**) to 1,2,4-TzNHC (**10**) as well as the substituents and their position on the N-phenyl wingtip. The electrochemical analysis revealed the shuttle electronic variations among the complexes and the complex **7** with *m*-Me-substituent has the maximum electron density at the Ru^{II}-center amongst the analyzed complexes. The effect of this electronic modulations was showcased in their catalytic performances in acceptorless dehydrogenation of 1-phenyl-1-propanol. The imidazolylidene complexes **2**-**9** were noted to be more active than the triazolylidene complex **10**. Among the imidazolylidene complexes, the reactivity pattern is significantly influenced by the position and nature of the substituents. We have also noted that under our reaction condition, this electronic modulation among the analogous *meta-* and *para*-substituted complexes has less effect on their activities in hydride transfer reaction. We believe that this study will help in designing and developing efficient catalytic systems for various fundamental and useful functional group transformations in synthetic chemistry.

4. Experimental section

4.1. Materials and method

All manipulations were performed under argon atmosphere using either standard Schlenk line or Glove box techniques unless otherwise stated. Glassware was dried at 130°C in an oven overnight before use. The solvents used for the synthesis were dried, distilled, and degassed by standard methods and stored over 4 Å molecular sieves. NMR measurements were performed on Bruker 400 and 500 MHz FT-NMR spectrometers. The chemical shifts in the ^{1}H NMR spectra were referenced to the residual proton signals of the deuterated solvents ($CDCl_3$, ^{1}H 7.26 ppm and $^{13}C\{^1H\}$ 77.16 ppm; DMSO-d_6, ^{1}H 2.50 ppm and $^{13}C\{^1H\}$ 39.52 ppm; CD_3CN, ^{1}H 1.94 ppm and $^{13}C\{^1H\}$ 1.32 and 118.26 ppm) and reported relative to TMS. Coupling constants are expressed in Hz. ESI-MS spectra were recorded with an Agilent 6545A Q-TOF Mass spectrometer and the electrochemical measurements were carried out with Metrohm autolab potentiostat/galvanostat MAC90009 instrument. The 3/4-substituted phenyl imidazoles, phenyl-1,2,4-triazole, $[Ru(p\text{-cymene})Cl_2]_2$ and 1-phenyl-1-propanol were synthesized according to the literature procedures [4b,7a,16]. All other chemicals were purchased from the commercial sources and used as received without further purification.

4.2. X-ray crystallography

X-ray data were collected on a Bruker APEX-II CCD diffractometer equipped with graphite-monochromated Mo Kα radiation (λ = 0.71073 Å) [17a]. Crystal was fixed at the tip of a glass fiber loop, and after mounting on the goniometer head, it was optically centered. The APEXII and APEXII-SAINT program were used for the data collection and unit cell determination, respectively [17a]. Processing of the raw frame data was performed using SAINT [17a,17b]. The structures were solved by SHELXT 2014/5 methods [17c] and refined against F2 using all reflections with the SHELXL-2014/7 (WinGX) program [17c,17d]. Non-hydrogen atoms were refined anisotropically. All hydrogen atoms were placed at the calculated positions. The crystallographic figures were generated by using *Mercury 4.2.0* programme.

4.3. Syntheses and characterizations

4.3.1. Synthesis of 3-ethyl-1-(p-tolyl)-1H-imidazol-3-ium bromide

(***1b***). To a pressure tube, compound **B** (0.684 g, 4.32 mmol), bromoethane (4.079 g, 37.43 mmol) and 6 mL of dry CH_3CN were added. The reaction mixture was then stirred at 90°C for 24 h. After that, the reaction mixture was allowed to attain room temperature. After decanting the solvent, the precipitated solid product was washed with diethyl ether and dried in vacuo. The product was obtained as colorless hygroscopic solid. Yield: 901 mg (3.36 mmol, 78.0%). ^{1}H NMR (400 MHz, $CDCl_3$) δ 10.84 (s, 1H), 7.76 (s, 1H), 7.69 (s, 1H), 7.63 (d, J = 8.1 Hz, 2H), 7.31 (d, J = 8.1 Hz, 2H), 4.63 (q, J = 7.3 Hz, 2H), 2.37 (s, 3H), 1.63 (t, J = 7.3 Hz, 3H) ppm. $^{13}C\{^1H\}$ NMR (101 MHz, $CDCl_3$) δ 140.6, 135.4, 132.1, 131.0, 123.1, 121.7, 120.9, 45.7, 21.2, 15.9 ppm.

4.3.2. Synthesis of 3-ethyl-1-(4-nitrophenyl)-1H-imidazol-3-ium bromide

(***1e***). A pressure tube was charged with compound **E** (0.204 gram, 1.075 mmol), bromoethane (1.02 gram, 9.31 mmol) and 6 mL of dry CH_3CN. This mixture was then allowed to stir at 90°C for 24 h. After cooling, the solvent was decanted and the obtained solid was washed with diethyl ether before drying in vacuo to get an air stable yellow powder. Yield: 243 mg (0.812 mmol, 76.0%). ^{1}H NMR (400 MHz, DMSO-d_6) δ 10.11 (s, 1H), 8.50 (m, 3H), 8.14 (d, J = 7.8 Hz, 3H), 4.33 (q, J = 7.2 Hz, 2H), 1.53 (t, J = 7.2 Hz, 3H) ppm. $^{13}C\{^1H\}$ NMR (101 MHz, DMSO-d_6) δ 147.5, 139.4, 136.1, 125.6, 123.4, 122.9, 121.0, 45.0, 14.8 ppm.

4.3.3. Synthesis of 3-ethyl-1-(m-tolyl)-1H-imidazol-3-ium bromide

(***1f***). To a pressure tube compound **F** (500 mg, 3.16 mmol) and bromoethane (2.98 g, 27.37 mmol) and 6 mL of dry CH_3CN were added. The reaction mixture was stirred at 90°C for 24 h. A similar work up procedure to the previous case was followed to obtain the product as an off-white hygroscopic solid. Yield: 662 mg (2.47 mmol, 78.0%). ^{1}H NMR (500 MHz, $CDCl_3$) δ 10.90 (s, 1H), 7.75 (s, 1H), 7.69 (s, 1H), 7.58 (s, 1H), 7.55 (d, J = 8.1 Hz, 1H), 7.41 (t, J = 8.1 Hz, 1H), 7.29 (d, J = 7.6 Hz, 1H), 4.65 (q, J = 7.8, 2H), 2.43 (s, 3H), 1.64 (t, J = 7.8 Hz, 3H) ppm. $^{13}C\{^1H\}$ NMR (126 MHz, $CDCl_3$) δ 141.3, 135.9, 134.5, 131.2, 131.1, 130.5, 122.8, 122.5, 120.7, 119.0, 45.9, 21.4, 15.9 ppm.

4.3.4. Synthesis of 3-ethyl-1-(3-methoxyphenyl)-1H-imidazol-3-ium bromide

(***1g***). It was synthesized by following a similar procedure mentioned above using compound **G** (500 mg, 2.87 mmol) and bromoethane (2.5 g, 23 mmol) and obtained as hygroscopic, off-white

solid. Yield: 624 mg (2.10 mmol, 73.0%). ^{1}H NMR (400 MHz, $CDCl_3$) δ 11.02 (s, 1H), 7.79 (s, 2H), 7.44 (s, 1H), 7.41 (d, J = 8.2 Hz, 1H), 7.29 (m, 1H), 7.02 (d, J = 8.3 Hz, 1H), 4.63 (q, J = 7.2 Hz, 2H), 3.94 (s, 3H), 1.67 (t, J = 7.2 Hz, 3H) ppm. ^{13}C{^{1}H} NMR (101 MHz, $CDCl_3$) δ 161.2, 135.9, 135.5, 131.3, 122.7, 120.8, 116.8, 113.3, 107.3, 56.6, 45.8, 15.9 ppm.

4.3.5. Synthesis of 3-ethyl-1-(3-(trifluoromethyl)phenyl)-1H-imidazol-3-ium bromide

(***1h***). Using compound **H** (500 mg, 2.35 mmol) and bromoethane (2.0 mg, 19 mmol) following the similar procedure for **1g**, the imidazolium salt **1h** was isolated as air stable white solid. Yield: 672 mg (2.09 mmol, 89.0%). ^{1}H NMR (400 MHz, $CDCl_3$) δ 11.06 (s, 1H), 8.21 (s, 1H), 8.03 (s, 2H), 7.96 (s, 1H), 7.70 (d, J = 4.1 Hz, 2H), 4.59 (q, J = 7.3 Hz, 2H), 1.63 (t, J = 7.3 Hz, 3H) ppm. ^{13}C{^{1}H} NMR (101 MHz, $CDCl_3$) δ 135.9, 135.0, 132.9, 132.5, 131.6, 126.9, 125.9, 123.6, 121.1, 118.9, 45.9, 15.7 ppm.

4.3.6. Synthesis of 3-ethyl-1-(3-nitrophenyl)-1H-imidazol-3-ium bromide

(***1i***). Using compound **I** (500 mg, 2.64 mmol) and bromoethane (2.3 g, 21 mmol) following the similar procedure for **1g**, the imidazolium salt **1i** was isolated as air stable pale yellow solid. Yield: 590 mg (1.98 mmol, 75.0%). ^{1}H NMR (500 MHz, DMSO-d_6) δ 10.02 (s, 1H), 8.73 (s, 1H), 8.47 (s, 1H), 8.43 (d, J = 8.1 Hz, 1H), 8.29 (d, J = 7.3 Hz, 1H), 8.12 (s, 1H), 7.98 (t, J = 8.2 Hz, 1H), 4.32 (q, J = 7.2 Hz, 2H), 1.53 (t, J = 7.3 Hz, 3H) ppm. ^{13}C{^{1}H} NMR (126 MHz, DMSO-d_6) δ 148.4, 136.1, 135.6, 131.7, 128.4, 124.3, 123.1, 121.3, 117.4, 44.9, 14.8 ppm.

4.3.7. Synthesis of 4-ethyl-1-phenyl-1H-1,2,4-triazol-4-ium bromide

(***1j***). Using compound **J** (600 mg, 4.13 mmol) and bromoethane (3.6 g, 33 mmol) following the similar procedure for **1g**, the imidazolium salt **1j** was isolated as air stable white solid. Yield: 808 mg (3.18 mmol, 77%). ^{1}H NMR (400 MHz, $CDCl_3$) δ 12.17 (s, 1H), 9.54 (s, 1H), 8.02 (d, J = 7.7 Hz, 2H), 7.51 (q, J = 9.9, 8.3 Hz, 3H), 4.76 (q, J = 7.4 Hz, 2H), 1.72 (t, J = 7.4 Hz, 3H) ppm. ^{13}C{^{1}H} NMR (126 MHz, $CDCl_3$) δ 144.3, 140.9, 140.8, 134.9, 131.0, 130.4, 120.6, 44.8, 15.9 ppm.

4.4. General procedure for the synthesis of orthometalated Ru^{II}-complexes ***2, 6*** and ***7-10***

To a pressure tube equipped with a magnetic stirring bar, azolium salt (1 equiv.), [Ru(*p*-cymene)Cl_2]$_2$ (0.5 equiv.), Cs_2CO_3 (2 equiv.), NaBr (3 equiv.) were added along with dry THF and stirred for 24 h at 70°C. After cooling, the solvent was dried in high vacuo and the residue was dissolved in dichloromethane. The obtained dark brown suspension was then filtered through neutral alumina to get a clear yellow solution which was further concentrated and precipitated using *n*-hexane to get air and moisture stable yellow to orange solids.

4.4.1. Synthesis of complex ***3***

Using the imidazolium salt **1b** (100 mg, 0.32 mmol), the general procedure was followed and the complex **3** was isolated as a pale-yellow solid. Yield 112 mg (0.22 mmol, 70.0%) ^{1}H NMR (400 MHz, $CDCl_3$) δ 7.91 (s, 1H), 7.32 (s, 1H), 7.00 (s, 1H), 6.95 (d, J = 7.8 Hz, 1H), 6.73 (d, J = 7.7 Hz, 1H), 5.54 (dd, J = 9.9, 6.0 Hz, 2H), 5.41 (d, J = 5.9 Hz, 1H), 5.33 (d, J = 5.8 Hz, 1H), 4.58 (dt, J = 14.0, 7.3 Hz, 1H), 4.47 (dd, J = 13.7, 7.2 Hz, 1H), 2.35 (s, 3H), 2.30–2.17 (m, 1H), 2.13 (s, 2H), 1.62 (t, J = 7.3 Hz, 3H), 0.91 (d, J = 6.9 Hz, 3H), 0.76 (d, J = 6.9 Hz, 3H) ppm. ^{13}C{^{1}H} NMR (101 MHz, $CDCl_3$) δ 186.5, 162.1, 143.3, 142.7, 133.4, 123.0, 119.6, 114.5, 110.6, 103.6, 99.8, 92.3, 89.9, 87.3, 84.0, 45.6, 31.2, 23.1, 21.9, 21.6, 19.7, 16.8 ppm.

4.4.2. Synthesis of complex ***6***

Using the imidazolium salt **1e** (100 mg, 0.32 mmol), the general procedure was followed and the complex **6** was isolated as an orange solid. Yield 132 mg (0.25 mmol, 78.0%). ^{1}H NMR (400 MHz, $CDCl_3$) δ 8.94 (s, 1H), 7.87 (d, J = 8.4 Hz, 1H), 7.41 (s, 1H), 7.12 (d, J = 8.6 Hz, 1H), 7.09 (s, 1H), 5.66 (d, J = 5.8 Hz, 1H), 5.62 (d, J = 5.5 Hz, 1H), 5.55 (d, J = 5.8 Hz, 1H), 5.39 (s, J = 5.8 Hz, 1H), 4.59 (dd, J = 14.0, 7.0 Hz, 1H), 4.48 (dd, J = 13.7, 7.1 Hz, 1H), 2.24 (m, 1H), 2.18 (s, 3H), 1.65 (t, J = 7.3 Hz, 3H), 0.91 (d, J = 6.8 Hz, 3H), 0.75 (d, J = 6.8 Hz, 3H) ppm. ^{13}C{^{1}H} NMR (101 MHz, $CDCl_3$) δ 189.2, 164.7, 150.9, 143.8, 136.3, 121.1, 119.4, 115.3, 110.5, 105.3, 101.4, 93.2, 90.8, 88.6, 84.5, 46.0, 31.3, 23.1, 21.9, 19.7, 16.7 ppm.

4.4.3. Synthesis of complex ***7***

Using the imidazolium salt **1f** (100 mg, 0.374 mmol), the general procedure was followed and the complex **7** was isolated as a yellow solid. Yield 148 mg (0.29 mmol, 79.0%). ^{1}H NMR (500 MHz, $CDCl_3$) δ 7.95 (d, J = 7.5 Hz, Ar-H, 1H), 7.34 (s, 1H), 7.00 (d, J = 2.0 Hz, Imidazole-H, 1H), 6.90 (s, 1H), 6.79 (d, J = 7.5 Hz, Ar-H, 1H), 5.56 (d, J = 6.0 Hz, *p*-cymene−Ph,1H), 5.52 (d, J = 6.5 Hz, *p*-cymene−Ph, 1H), 5.39 (d, J = 6.0 Hz, *p*-cymene−Ph, 1H), 5.30 (d, J = 6.5 Hz, *p*-cymene−Ph, 1H), 4.58 (dq, J = 14.7, 7.4 Hz, N$\underline{CH_2}$CH$_3$, 1H), 4.48 (dq, J = 14.6, 7.3 Hz, N$\underline{CH_2}$CH$_3$, 1H), 2.33 (s, Ph-Me, 3H), 2.26 (sept, J = 6.9 Hz, *p*-cymene−*i*Pr, 1H), 2.12 (s, *p*-cymene−Me, 3H), 1.62 (t, J = 7.4 Hz, NCH$_2\underline{CH_3}$, 3H), 0.93 (d, J = 6.9 Hz, *p*-cymene−*i*Pr, 3H), 0.77 (d, J = 6.9 Hz, *p*-cymene−*i*Pr, 3H) ppm. ^{13}C{^{1}H} NMR (126 MHz, $CDCl_3$) δ 187.2, 157.6, 145.4, 141.6, 131.7, 125.5, 119.6, 114.5, 112.2, 103.0, 100.2, 92.4, 89.9, 87.4, 83.7, 45.7, 31.2, 23.2, 21.8, 21.2, 19.7, 16.8 ppm.

4.4.4. Synthesis of complex ***8***

Using the imidazolium salt **1h** (100 mg, 0.311 mmol), the general procedure was followed and the complex **8** was isolated as a dark yellow solid. Yield: 140 mg (0.25 mmol, 80.0%). ^{1}H NMR (500 MHz, $CDCl_3$) δ 8.21 (d, J = 7.7 Hz, Ar-H, 1H), 7.41 (s, 1H), 7.24 (s, 1H), 7.17 (d, J = 7.7 Hz, Ar-H, 1H), 7.06 (s, 1H), 5.58 (m, J = 4.6 Hz, *p*-cymene−Ph, 2H), 5.46 (d, J = 6.0 Hz, *p*-cymene−Ph, 1H), 5.36 (d, J = 5.9 Hz, *p*-cymene−Ph, 1H), 4.58 (dq, J = 14.5, 7.4 Hz, N$\underline{CH_2}$CH$_3$, 1H), 4.48 (dq, J = 14.2, 7.2 Hz, N$\underline{CH_2}$CH$_3$, 1H), 2.24 (m, J = 6.9 Hz, *p*-cymene−*i*Pr, 1H), 2.14 (s, *p*-cymene−Me, 3H), 1.63 (t, J = 7.3 Hz, NCH$_2\underline{CH_3}$, 3H), 0.92 (d, J = 6.9 Hz, *p*-cymene−*i*Pr, 3H), 0.76 (d, J = 6.8 Hz, *p*-cymene−*i*Pr, 3H) ppm. ^{13}C{^{1}H} NMR (126 MHz, $CDCl_3$) δ 187.5, 170.1, 145.7, 142.0, 120.6 (q, J = 3.5 Hz), 120.4, 114.8, 107.2 (q, J = 3.5 Hz), 104.3, 101.2, 92.7, 90.6, 88.2, 84.4, 45.8, 31.2, 23.1, 21.8, 19.7, 16.8 ppm. ^{19}F {^{1}H}NMR (471 MHz, $CDCl_3$) δ -61.35 (s) ppm.

4.4.5. Synthesis of complex ***9***

Using the imidazolium salt **1i** (100 mg, 0.335 mmol), the general procedure was followed and the complex **8** was isolated as a brown solid. Yield: 122 mg (0.23 mmol, 69.0%). ^{1}H NMR (500 MHz, $CDCl_3$) δ 8.27 (d, J = 8.2 Hz, Ar-H, 1H), 7.89 (d, J = 2.2 Hz, Imidazole-H, 1H), 7.82 (dd, J = 8.2, 2.2 Hz, 1H), 7.48 (d, J = 2.1 Hz, 1H), 7.11 (d, J = 2.1 Hz, 1H), 5.64 (m, 2H), 5.52 (d, J = 5.5 Hz, *p*-cymene−Ph,1H), 5.40 (d, J = 5.9 Hz, *p*-cymene−Ph, 1H), 4.57 (dq, J = 14.8, 7.4 Hz, N$\underline{CH_2}$CH$_3$, 1H), 4.47 (dq, J = 14.6, 7.3 Hz, N$\underline{CH_2}$CH$_3$,1H), 2.24 (m, *p*-cymene−*i*Pr, 1H), 2.17 (s, *p*-cymene−Me,3H), 1.65 (t, J = 7.4 Hz, NCH$_2\underline{CH_3}$, 3H), 0.91 (d, J = 6.9 Hz, *p*-cymene−*i*Pr, 3H), 0.75 (d, J = 6.9 Hz, *p*-cymene−*i*Pr, 3H) ppm. ^{13}C{^{1}H} NMR (126 MHz, $CDCl_3$) δ 187.6, 181.1, 145.9, 144.4, 141.9, 120.9, 118.6, 115.1, 105.7, 105.2, 101.8, 93.31, 91.2, 89.0, 85.0, 45.9, 31.2, 23.1, 21.9, 19.7, 16.7 ppm.

4.4.6. Synthesis of complex ***10***

Using the imidazolium salt **1j** (100 mg, 0.393 mmol), the general procedure was followed and the complex **10** was isolated as a

dark yellow solid. Yield 132 mg (0.27 mmol, 69.0%). ^{1}H NMR (500 MHz, $CDCl_3$) δ 8.08 (m, 1H), 8.04 (s, 1H), 7.46 (m, 1H), 7.01 (m, 2H), 5.69 (d, J = 6.0 Hz, 1H), 5.62 (d, J = 5.9 Hz, 1H), 5.44 (d, J = 6.0 Hz, 1H), 5.32 (d, J = 5.9 Hz, 1H), 4.59 (dq, J = 14.0, 7.5 Hz, 1H), 4.48 (dt, J = 14.0, 7.1 Hz, 1H), 2.32 (p, J = 6.9 Hz, 1H), 2.13 (s, 2H), 1.69 (t, J = 7.3 Hz, 3H), 0.95 (d, J = 6.9 Hz, 2H), 0.77 (d, J = 6.8 Hz, 2H) ppm. ^{13}C{^{1}H} NMR (126 MHz, $CDCl_3$) δ 189.3, 159.6, 144.7, 141.6, 140.9, 125.4, 122.7, 112.8, 103.4, 102.0, 92.8, 90.4, 88.0, 83.6, 43.7, 31.3, 23.1, 21.9, 19.7, 16.5 ppm.

4.5. General procedure of the catalytic experiments

4.5.1. Catalytic acceptorless dehydrogenation of 1-phenyl-1-propanol

Catalyst (0.5/0.3 mol%) from a stock solution, prepared by dissolving the required amount of the complex in acetonitrile, was added to a predried Schlenk tube (25 mL) equipped with a magnetic stirring bar and the acetonitrile was then dried in high vacuo. After that, KO^{t}Bu (0.2 equiv.) followed by 1-phenyl-1-propanol (0.5 mmol) and dry toluene were added. The reaction mixture was then heated to reflux under open condition for the specified time. The reaction mixture was then cooled, a 25 μL aliquot was then taken and diluted with 1 mL of methanol to determine the conversion using GC-MS.

4.5.1. Catalytic transfer hydrogenation of acetophenone

Catalyst (0.25/0.1 mol%), KO^{t}Bu (0.1 equiv.) and acetophenone (1 mmol) were added to an oven dried pressure tube (25 mL) and heated to reflux for specified time. The reaction mixture was then cooled, a 25 μL aliquot was then taken and diluted with 1 mL of methanol to determine the conversion using GC-MS.

Declaration of Competing Interest

The authors declare that they have no known competing financial interests or personal relationships that could have appeared to influence the work reported in this paper.

Acknowledgments

We gratefully acknowledge DST and SERB, India (Project No. DST/INSPIRE/04/2015/002219 and CRG/2020/000780, respectively) for the financial support. P.M.I and V.K.S thank IIT Madras for the research fellowship. We gratefully acknowledge the NMR and ESI-MS (DST-FIST funded) facility at the Department of Chemistry, IIT Madras, single-crystal X-ray diffractometer facility at the Department of Chemistry and SAIF, IIT Madras, and Dr. K.R.R.'s laboratory for the CV and DPV measurements. We sincerely thank Prof. F. E. Hahn for the crystal measurements of **1i** and **10**.

Supplementary materials

Supplementary material associated with this article can be found, in the online version, at doi:10.1016/j.jorganchem.2021.122008.

References

[1] A.J. Arduengo, R.L. Harlow, M. Kline, J. Am. Chem. Soc. 113 (1991) 361–363.
[2] (a) R.H. Crabtree, J. Organomet. Chem. 690 (2005) 5451–5457; (b) F.E. Hahn, M.C. Jahnke, Angew. Chem. Int. Ed. 47 (2008) 3122–3172; (c) H.V. Huynh, Chem. Rev. 118 (2018) 9457–9492; (d) T.T. Dang, B. Ramalingam, S.P. Shan, A.M. Seayad, ACS Catal 3 (2013) 2536–2540.
[3] (a) M.N. Hopkinson, C. Richter, M. Schedler, F. Glorius, Nature 510 (2014) 485–496; (b) M. Huang, J. Liu, Y. Li, X.-B. Lan, P. Su, C. Zhao, Z. Ke, Catal. Today 370 (2021) 114–141; (c) L.-A. Schaper, S.J. Hock, W.A. Herrmann, F.E. Kühn, Angew. Chem. Int. Ed. 52 (2013) 270–289; (d) C.M. Crudden, D.P. Allen, Coord. Chem. Rev. 248 (2004) 2247–2273.
[4] (a) E. Peris, R.H. Crabtree, Coord. Chem. Rev. 248 (2004) 2239–2246; (b) S.N.R. Donthireddy, P.M. Illam, A. Rit, Inorg. Chem. 59 (2020) 1835–1847; (c) D.A. Hey, R.M. Reich, W. Baratta, F.E. Kühn, Chem. Rev. 374 (2018) 114–132; (d) H. Ohara, W.N.O. Wylie, A.J. Lough, R.H. Morris, Dalton Trans 41 (2012) 8797–8808.
[5] F.E. Fernández, M.C. Puerta, P. Valerga, Organometallics 31 (2012) 6868–6879.
[6] (a) S.K. Gupta, S.K. Sahoo, J. Choudhury, Organometallics 35 (2016) 2462–2466; (b) S. Semwal, I. Mukkatt, R. Thenarukandiyil, J. Choudhury, Chem. Eur. J. 23 (2017) 13051–13057.
[7] (a) S. Bauri, S.N.R. Donthireddy, P.M. Illam, A. Rit, Inorg. Chem. 57 (2018) 14582–14593; (b) P.M. Illam, S.N.R. Donthireddy, S. Chakrabartty, A. Rit, Organometallics 38 (2019) 2610–2623; (c) J. Soellner, I. Císařová, T. Strassner, Organometallics 37 (2018) 4619–4629.
[8] (a) X. Xie, H.V. Huynh, Org. Chem. Front. 2 (2015) 1598–1603; (b) D. Schleicher, H. Leopold, H. Borrmann, T. Strassner, Inorg. Chem. 56 (2017) 7217–7229.
[9] (a) S. Hitzel, C. Farber, C. Bruhn, U. Siemeling, Organometallics 33 (2014) 425–428; (b) S. Bauri, A. Mallik, A. Rit, Organometallics 39 (2020) 3362–3374.
[10] D. Schleicher, A. Tronnier, H. Leopold, H. Borrmann, T. Strassner, Dalton Trans 45 (2016) 3260–3263.
[11] (a) C. Gunanathan, D. Milstein, Science 314 (2013) 1229712; (b) M. Maji, D. Panja, I. Borthakur, S. Kundu, Org. Chem. Front. 8 (2021) 2673–2709.
[12] (a) S.N.R. Donthireddy, C.S. Tiwari, S. Kumar, A. Rit, Asian J. Org. Chem. 10 (2021) 464–484; (b) V.K. Singh, S.N.R. Donthireddy, P.M. Illam, A. Rit, Dalton Trans 49 (2020) 11958–11970; (c) S.N.R. Donthireddy, V.K. Pandey, A. Rit, J. Org. Chem. 86 (2021) 6994–7001.
[13] (a) S. Shahane, C. Fischmeister, C. Bruneau, Catal. Sci.Technol. 2 (2012) 1425–1428; (b) W. Chang, X. Gong, S. Wang, L.-P. Xiao, G. Song, Org. Biomol. Chem. 15 (2017) 3466–3471; (c) F.P. Malan, E. Singleton, P.H. van Rooyen, M. Albrecht, M. Landman, Organometallics 38 (2019) 2624–2635; (d) J. De-Pasquale, M. Kumar, M. Zeller, E.T. Papish, Organometallics 32 (2013) 966–979; (e) X. Xie, H.V. Huynh, ACS Catal 5 (2015) 4143–4151.
[14] J.A. Widegren, R.G. Finke, J. Mol. Catal. A: Chem. 198 (2003) 317–341.
[15] (a) S. Burling, B.M. Paine, D. Nama, V.S. Brown, M.F. Mahon, T.J. Prior, P.S. Pregosin, M.K. Whittlesey, J.M.J. Williams, J. Am. Chem. Soc. 129 (2007) 1987–1995; (b) K. Farrell, H. Müller-Bunz, M. Albrecht, Dalton Trans 45 (2016) 15859–15871; (c) L. Mercs, A. Neels, H. Stoeckil-Evans, M. Albrecht, Inorg. Chem. 50 (2011) 8188–8196.
[16] M.A. Bennett, A.K. Smith, J. Chem. Soc., Dalton Trans. (1974) 233–241.
[17] (a) SADABS, v 2.05, Bruker AXS Inc., Madison, WI, 2003; (b) G.M. Sheldrick, SAINT, version 8.37A, 2013 Bruker AXS Inc, WI; (c) G.M. Sheldrick, 2015 Acta Crystallogr., Sect. A: Found. Adv., 71 3–8; (d) L.J. Farrugia, 2012 J. Appl. Crystallogr., 45 849–854.